# $Co_3O_4/CuMoO_4$ Hybrid Microflowers Composed of Nanorods with Rich Particle Boundaries as a Highly Active Catalyst for Ammonia Borane Hydrolysis

Dongsheng Lu,[a] Jinyun Liao,[a] Hao Li,*[a], Shan Ji,*[b] and Bruno G. Pollet [c]

[a] *School of chemistry and Materials Engineering, Huizhou University, No.46, Yada Avenue, Huizhou 516007, China.*

[b] *College of Biological, Chemical Science and Chemical Engineering, No.56, Yuexiunan Road, Jiaxing University, Jiaxing, 314001, China.*

[c] *Department of Energy and Process Engineering, Faculty of Engineering, Norwegian University of Science and Technology. No-7491 Trondheim, Norwegian.*

Corresponding Authors

E-mail: lihao180@126.com (H. Li).

E-mail: jishan@mail.zjxu.edu.cn (Shan Ji).

**Abstract:** Dehydrogenation of ammonia borane (AB) is a promising approach for the production and use of hydrogen for industrial and fuel cell applications. The development of low-cost and highly active catalysts is critical for these practical applications. In this study, low-cost $Co_3O_4/CuMoO_4$ hybrid microflowers composed of nanorods with rich particle boundaries were synthesized. $Co_3O_4/CuMoO_4$ was used as a catalyst for the dehydrogenation of AB and showed a high catalytic activity with a turnover frequency (TOF) of 129.15 $mol_{hydrogen}mol_{cat}^{-1}$ $min^{-1}$ at room temperature. The apparent activation energy (Ea) of the catalyst was found to be as low as 23.2 kJ $mol^{-1}$. It was revealed that the synergistic effect between $Co_3O_4$ and $CuMoO_4$ played a critical role in improving the catalytic activity. $Co_3O_4$ is relatively active, but a long induction time is needed when it acts as a catalyst in AB hydrolysis. In contrast, $CuMoO_4$ is less active, but it can immediately catalytically initiate the hydrolytic reaction. When these two compound are combined as a hybrid catalyst, its catalytic performance is significantly improved. These findings can provide

some new insight for those who are trying to design some noble-metal-free hybrid catalyst with high catalytic activity towards AB hydrolysis.

**Keywords:** Microflowers; Hydrolysis; Ammonia borane; Hydrogen production.

## Introduction

Hydrogen is regarded as a "clean" energy source when it is used in a fuel cell, in which chemical energy can directly be converted to electrical energy with high efficiency.[1-4] The energy density of hydrogen (120 kJ $g^{-1}$) is ca. 3 times as high as that of petroleum (44 kJ $g^{-1}$), allowing it to be a perfect "fuel" for mobile and stationary applications.[5] With the rapid development of proton exchange membrane fuel cell (PEMFC) and other fuel cell-based hydrogen systems in various market sectors, a huge demand in hydrogen production and storage is required. Recently, the production of hydrogen from chemical hydrogen-storage materials, such as sodium borohydride ($NaBH_4$), formic acid (HCOOH) and ammonia borane ($NH_3BH_3$, AB), has been proven to be a feasible and effective approach for practical applications.[6,7] For example, in the presence of a suitable catalyst, 1 mole of $NaBH_4$ can generate 4 moles of pure di-hydrogen ($H_2$) via hydrolysis. So far, precious group metals (PGM), such as Rh,[8] Ru,[9] Pd,[10] PdAg,[11-12] PtCu[13] and Pt[14] are effective catalysts for the hydrolysis of $NaBH_4$, HCOOH and AB, but their high cost and scarcity significantly impede their use in industrial and domestic applications. In the last few years, the development of alternative catalysts to replace expensive PGMs for catalytic hydrolysis has attracted tremendous attention.

On the other hand, the hydrogen content of AB (19.6 wt.%) is much higher than those of $NaBH_4$ (10.8 wt.%) and HCOOH (4.3 wt.%), which have attracted extensive interests in recent years. Many researchers have demonstrated that some cheap metal/alloy catalysts, such as Co,[15] Cu,[16] Ni,[17] CoCu,[18] Ni-Co-P[19] and Co-W-B[20] are active to AB hydrolysis. However, the catalytic activity of these transition metal or alloy catalysts is still not high enough to guarantee the fast hydrogen

production in most cases. Thus, it is highly desirable to develop other types of catalysts with both low cost and high performance towards AB. Over the past several years, nanocomposites of different transitional metal oxides or hydroxides emerge as a novel type of heterogeneous catalysts to AB hydrolysis. For example, Feng et al. have reported CuO-CoO nanoparticles deposited on graphene oxide as hybrid catalysts for dehydrogenation of AB, which exhibit an initial turnover frequency (TOF) of 70.0 $mol_{hydrogen}mol_{cat}^{-1}$ $min^{-1}$.[21] Yamada et al. have designed $Cu_2O$-$Co_3O_4$ composites by decorating $Cu_2O$ particles with $Co_3O_4$ nanoparticles, which can protect $Cu_2O$ particles from agglomeration, resulting in the high catalytic performance.[22] CuO-NiO nanocomposites have been proved by Yen et al. to be a robust catalyst towards AB hydrolysis with the TOF of 60 $mol_{hydrogen}mol_{Cu}^{-1}$ $min^{-1}$. Very recently, Peng et al. have tested the catalytic activity of the $Cu(OH)_2/Fe(OH)_3$ nanocomposite in AB hydrolysis and they find the corresponding TOF can reach 50.3 $mol_{hydrogen}mol_{cat}^{-1}$ $min^{-1}$, which is superior to those of previously reported Fe or Cu based systems.[24] It seems to be a feasible way to improve the catalytic activity by compositing different transitional metal oxides or hydroxides. However, what is the role of the each component of the composite in AB hydrolysis? Is there any synergetic effect between the different transitional metal-based compounds in AB hydrolysis? To address these issues, further investigation is still necessary.

Very recently, we have synthesized yolk-shell $Co_3O_4$ microspheres, which exhibit high catalytic activity in AB hydrolysis when they are decorated with Cu (Ⅱ).[25] On the other hand, Mo oxide species can serve as Lewis acid sites, which is favorable for the hydrolytic reaction of AB.[26] Thus, it is likely that the composites of $Co_3O_4$ and $CuMoO_4$ exhibit high catalytic activity in AB hydrolysis. Motivated by this idea, $Co_3O_4/CuMoO_4$ hybrid microflowers composed of nanorods are prepared and acted as catalysts for the hydrolysis of AB in this work. As far as we know, such catalysts towards AB hydrolysis for hydrogen production have not been reported yet. It is found that the nanorods in the $Co_3O_4/CuMoO_4$ hybrid microflowers contain rich grain boundaries. More importantly, there is a significant synergistic effect between $Co_3O_4$ and $CuMoO_4$. The as-obtained

$Co_3O_4/CuMoO_4$ hybrid materials exhibited high catalytic activity with a TOF value of 129.15 $mol_{hydrogen}mol_{cat}^{-1}$ $min^{-1}$ for the hydrolysis of AB, which was found to be superior to most of noble-metal-free catalysts in the literature.

## Experimental

### Preparation of catalysts

All reagents were of analytic grade (AR) and directly used in all experiments without any further purification. The detail procedure of preparing $Co_3O_4/CuMoO_4$ was as follows: $Co(NO_3)_2 \cdot 6H_2O$ (4.5 mmol), $C_6H_{12}N_4$ (2.25 mmol) and $Na_3C_6H_5O_7 \cdot 2H_2O$ (1.5 mmol) were dissolved in 35 mL of water. The obtained solution was transferred into a Teflon-lined stainless-steel autoclave and heated to 100 $^oC$ for 24 h. The obtained product was filtered out and washed with water, and then dried in a vacuum oven at 40 $^oC$ for 12 h. 4 samples of the dried products (90 mg for each) were weighed and transferred in 4 different beakers containing 40 mL water in each of them. Subsequently, 0.25, 0.5, 1.0, 2.0 mmol of $CuCl_2$ and $H_2MoO_4$ (molar ratio is 1:1) mixtures were added into the above 4 solutions, and then 2.5, 5.0, 10.0, 20.0 mmol of urea were dissolved in the 40 mL ultrapure water, they were added into these 4 solutions respectively. The obtained solutions were stirred for 30 min, transferred into Teflon-lined stainless-steel autoclaves and then heated at 160 $^oC$ for 8 h. After the autoclaves were cooled to room temperature, the obtained products were filtered out, rinsed with water and dried in vacuum oven at 40 $^oC$. The dried products were heated at 500 $^oC$ for 2 h (heating temperature rate of 2 $^oC$ $min^{-1}$). The final products were obtained after the heat-treatment and labelled as Co/Cu-X (X: represents the concentration in mmol of the mixtures of $CuCl_2$ and $H_2MoO_4$).

### Characterization

X-Ray diffraction (XRD) patterns were recorded using a PANalytical B.V. Empyean X-ray diffractometer with CuK radiation ( $\lambda$ = 1.5406 Å). The surface morphology of the film catalyst was studied using a Carl Zeiss Ultra Plus scanning electron microscope (SEM). The specific surface

area was determined by the Brunauer-Emmett-Teller (BET) method based upon the sorption isotherms obtained on a Quantachrome Autosorb-1 volumetric analyzer. Transmission electron microscope (TEM) and high-resolution transmission electron microscope (HRTEM) images were obtained on a FEI Tecnai G2 F20 high-resolution transmission electron microscope operating at 200 kV. $H_2$ temperature-programmed reduction ($H_2$-TPR) experiment was performed by using an automatic chemisorption analyzer (TP5080) equipped with a thermal conductivity detector (TCD). In this process, approximately 100 mg of the sample was treated with a 50 mL $min^{-1}$ stream of 10 vol% $H_2$ in argon from ambient temperature to 800 $^oC$ at a heating temperature rate of 10 $^oC$ $min^{-1}$. The molar ratios of $Co_3O_4$ to $CuMoO_4$ in different samples were determined with an Agilent 7800 ICP-MASS. The Fourier transform infrared spectra (FTIR) were recorded on a Bruker TENSOR27 FTIR spectrophotometer. X-ray photoelectron spectroscopy (XPS) measurement was performed with PHI 5000 Versa Probe.

**Catalytic experiments**

The catalytic hydrolysis of AB was carried out in a three-necked glass container connected with a gas burette to measure the accumulative volume of $H_2$ generated during the hydrolysis reaction. Typically, 3 mmol AB and 20 mmol NaOH were mixed into the reaction vessel containing 20 mL of ultrapure water, followed by the addition of 10 mg of the catalyst under ultrasonication. The reaction temperature was set at 25 $^oC$ using a thermostatic bath. For the purpose of testing the reusability and recyclability of the catalysts, we repetitively added the equal amount of AB to the solution after the previous catalytic run is over, and recorded hydrogen volume as described above.

## Results and discussion

The morphology of the obtained samples were investigated by SEM and their corresponding SEM images are presented in Figure 1(a-e). As shown in Figure 1(a), the Co/Cu-0.25 is three-dimensional flower-like microspheres consisting of many nanorods and nanoparticles. When the amount of $CuCl_2$ and $H_2MoO_4$ increased in the precursors, only regular nanorods with a diameter of 50-100 nm were observed in the microflowes, as shown in the SEM images (Figure 1

(b-e)). The detailed structure of Co/Cu-0.5 was further evaluated by TEM. As shown in Figure 1(f), the obtained microflowers have an even diameter of ca. 2 μm and are composed of many fine nanorods. We selected a piece of nanorod (Figure 1(g)) in the microflower and carried out elemental mapping analysis on it. As presented in Figure 1(h-k), Co, Mo, Cu and O are uniformly distributed in the nanorod. High-resolution TEM (HR-TEM) image of the Co/Cu-0.5 sample in Figure 1(l) clearly displays a rough, turf and rich particle boundaries, made of irregular small nanoparticles. The HR-TEM image also clearly shows well-defined lattice fringes on the Co/Cu rod. The d-spacing distances were measured to be 0.28 nm and 0.23 nm, corresponding to the (220) crystal plane of $Co_3O_4$ and (-201) plane of $CuMoO_4$ respectively.

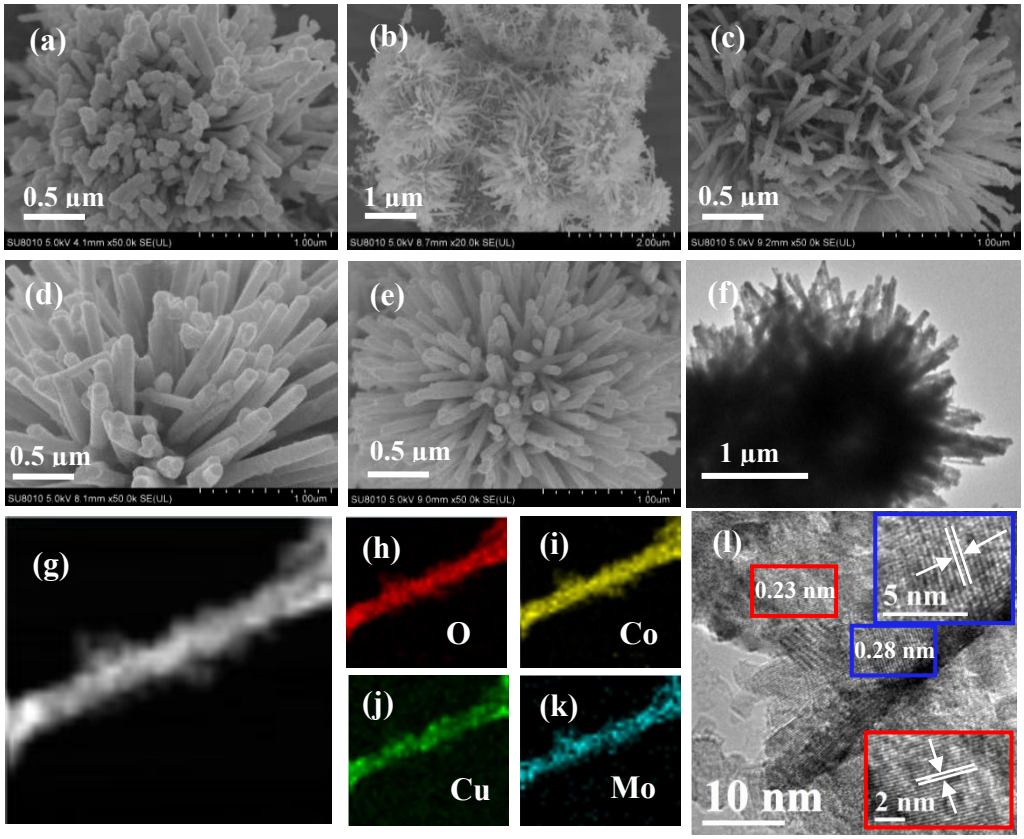


Figure 1 SEM images of Co/Cu-0.25 (a), Co/Cu-0.5 (b-c), Co/Cu-1(d), Co/Cu-2 (e); TEM images of Co/Cu-0.5 (f); Elemental mapping analysis of Co/Cu-0.5 (g-k); (l) HRTEM images of Co/Cu-0.5.

The crystallinity of the obtained Co/Cu-X samples were studied by X-ray diffraction analysis, as

shown in Figure 2. All the XRD patterns show similar features, i.e. only weak and wide peaks were observed. When benchmarked with the standard XRD pattern of $Co_3O_4$ (JCPDS 43-1003) and $CuMoO_4$ (JCPDS 47-0511), the characteristic peaks of $Co_3O_4$ (JCPDS 43-1003) are found at 2 θ of 31.27°, 36.84°, 44.80°, 59.35° and 65.23° corresponding to the (220), (311), (400), (511) and (440) planes respectively for all four samples. It was also found that the diffraction peaks of CuMoO4 (JCPDS 47-0511) correspond to (012), (-201) and (2-20) planes in all four XRD patterns. The XRD results indicate that $Co_3O_4$ and $CuMoO_4$ with low crystallinity were formed in these Co/Cu-X samples. Nitrogen ($N_2$) sorption analysis was adopted to investigate the specific surface area of these obtained Co/Cu samples. $N_2$ sorption plots of all the Co/Cu samples exhibit IUPAC type III isotherms, without obvious hysteresis loop, indicating the existence of mesopores. Based on the $N_2$ sorption results, the calculated BET surface area of Co/Cu-0.25, Co/Cu-0.5, Co/Cu-1, and Co/Cu-2 samples were 77.2, 55.1, 51.6 and 47.9 $m^2$ $g^{-1}$, respectively (Figure S1). To clarify the compositions of the samples, ICP-MASS analysis were carried out. According to the results, the molar ratio of $Co_3O_4$ to $CuMoO_4$ is 1:1.11 for Co/Cu-0.25, 1:1.89 for Co/Cu-0.5, 1:2.61 for Co/Cu-1 and 1:4.5 for Co/Cu-2, respectively.

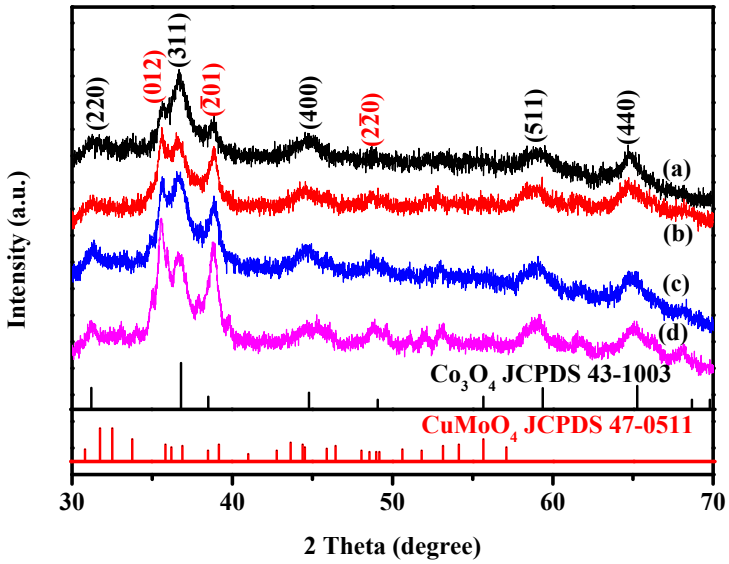


Figure 2 XRD patterns of (a) Co/Cu-0.25; (b) Co/Cu-0.5; (c) Co/Cu-1; (d) Co/Cu-2.

The hybrid features of Co/Cu-0.5 materials were further identified by FTIR spectrum as shown in

Figure 3. In the figure, the absorption peak at 557 and 655 $cm^{-1}$ can be assigned to the $Co_3O_4$ spinel oxide.[27] The peaks at 941 and 966 $cm^{-1}$ are attributed to the v1 vibration of distorted $MoO_6$ in $CuMoO_4$. The peaks in the range of 700-800 $cm^{-1}$ correspond to the stretching vibrations of Cu-O and Mo-O. The main bands emerged at 800-900 $cm^{-1}$ are due to the stretching vibrations of the Mo-O-Mo groups.[28] The FTIR results further confirm that there were $Co_3O_4$ and $CuMoO_4$ materials that co-existed in the tested sample.

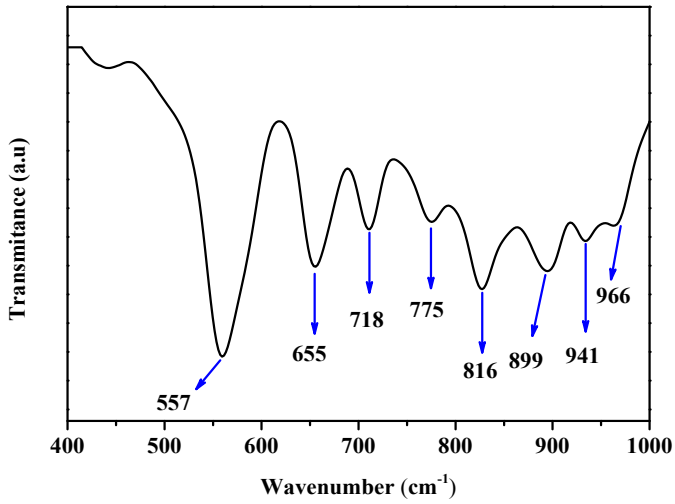


Figure 3 FTIR spectroscopy of Co/Cu-0.5.

The chemical composition and element state of Co/Cu-0.5 were evaluated by XPS analysis and presented in Figure 4. As shown in Figure 4(a), C, Cu, Co, Mo and O elements were found in the as-prepared sample. Figure 4(b) shows the Co 2p XPS spectrum, indicating that there are two peaks at 779.5 and 795.4 eV corresponding to Co 2p3/2 and Co 2p1/2 with two shake-up satellites.[29] The deconvoluted peaks at 796.6 and 781.2 eV can be ascribed to $Co^{2+}$ and the peaks at 779.6 and 794.8 eV can be indexed to $Co^{3+}$.[30] Figure 4(c) shows two main peaks at ca. 934.4 and 954.2 eV corresponding to Cu 2p3/2 and Cu 2p1/2 respectively indicating the presence of $Cu^{2+}$ in the sample. Figure 4(d) shows the Mo 3d XPS spectrum of Co/Cu-0.5, where two peaks at 232.6 and 235.7 eV correspond to the Mo 3d5/2 and Mo 3d3/2 of $Mo^{6+}$ respectively.[31] The XPS results confirmed that $Co^{2+}$, $Co^{3+}$, $Cu^{2+}$ and $Mo^{6+}$ existed on the surface of Co/Cu-0.5, which well match the chemical

states of elements of Co, Cu Mo in $Co_3O_4$/$CuMoO_4$. Meanwhile, we analyzed the surface composition of the Co/Cu-X samples by XPS and the results are displayed in Table S1. It is found that the molar ratios of $Co_3O_4$ to $CuMoO_4$ determined by XPS is very close to those determined by ICP-MASS for the Co/Cu-0.25 and Co/Cu-0.5, implying that $Co_3O_4$ and $CuMoO_4$ are quite uniformly distributed in these two samples. In contrast, pronounced composition deviations between two XPS and ICP-MASS analysis were observed for Co/Cu-1 and Co/Cu-2, hinting that $Co_3O_4$ and $CuMoO_4$ were imhomogeneously distributed as the Cu content increase in the samples.

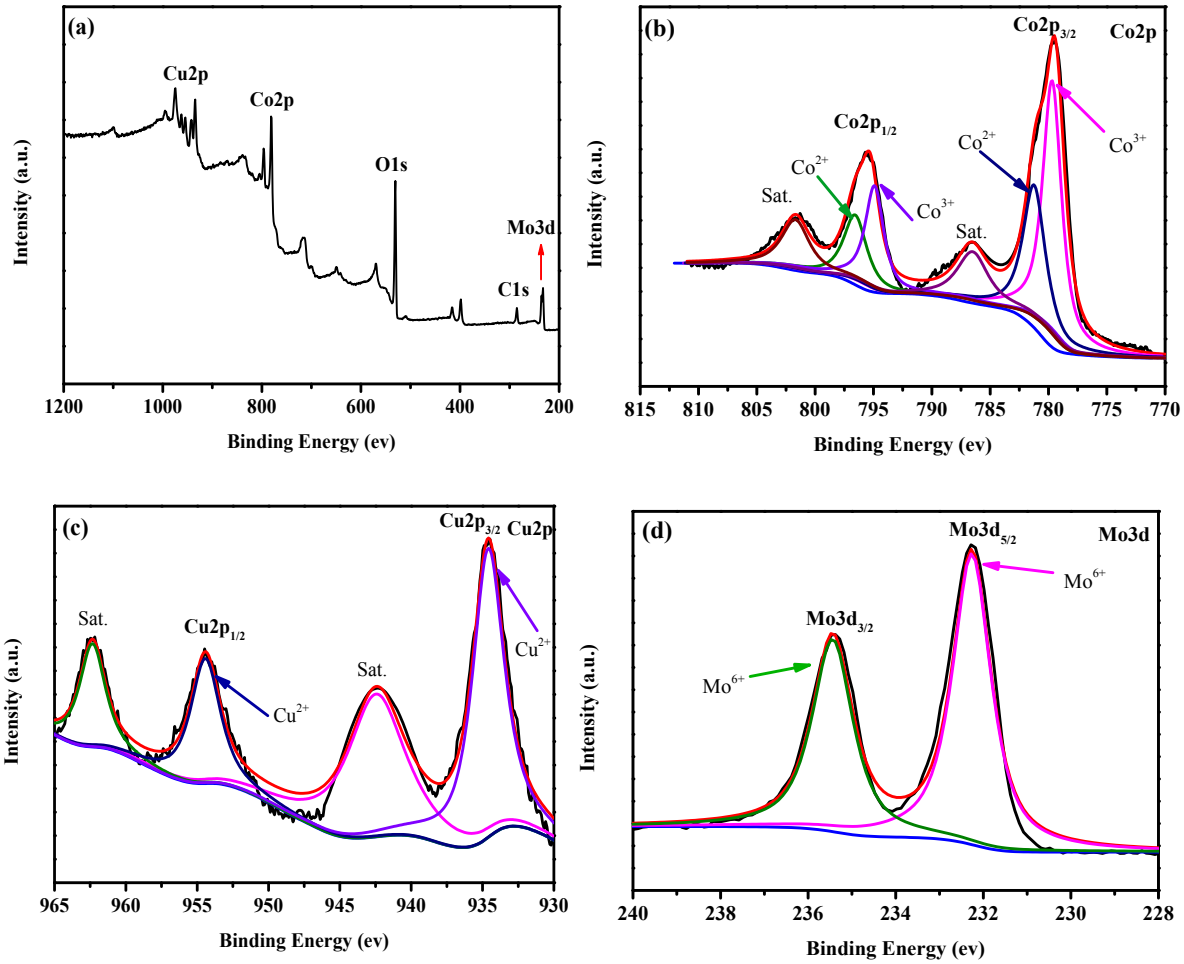


Figure 4 XPS spectrum of survey scan (a), deconvoluted high-resolution spectra of Co 2p (b), Cu 2p (c) and Mo 3d (d) for Co/Cu-0.5.

The catalytic performance of all the as-prepared samples was initially investigated by the hydrolysis of AB at 25 $^{o}$C; their corresponding hydrogen evolution curves are displayed in Figure

5(a). The figure shows that, except for the $CuMoO_4$ sample, the molar ratio of $H_2$ to AB can reach 3 for all other samples due to the complete hydrolysis of AB. It is worth noting that AB hydrolysis were carried out in the presence of NaOH in the present study. For comparison, we carried out a catalytic experiment in the absence of NaOH and corresponding hydrogen evolution curve is shown in Figure S2. Clearly, it will take a long time (about 12 minutes) to complete the hydrolytic reaction when Co/Cu-0.5 acts a catalyst, indicating that NaOH can promote AB hydrolysis. This result is in a good agreement with that in previous report.[32] Usually, the catalytic activity of hydrolysis can be evaluated by the TOF value. According to the literature, [33] the TOF value for a catalyst in AB hydrolysis can be calculated by following equation:

$$\mathrm{TOF} = \frac{\mathrm{n(H_2)}}{\mathrm{n(cat.)} \cdot \mathrm{t}}$$

Herein, $n(H_2)$, n(cat.) and t is the mole number of generated hydrogen (mol), mole number of the catalyst (mol) used in AB hydrolysis and the reaction time (min), respectively. The TOF values for these samples were calculated based upon the data taken from the linear part of the curves in Figure 5(a). Figure 5(b) displays the TOF values of Co/Cu-X, $Co_3O_4$ and $CuMoO_4$. The TOF values of $Co_3O_4$ and $CuMoO_4$ are quite low, which are19.35 and 3.49 $mol_{hydrogen}mol_{cat}^{-1}$ $min^{-1}$, respectively. It should be mentioned that an induction period (about 7 min) is observed for $Co_3O_4$ and nearly no hydrogen is produced during that period. We do not take the induction time into consideration when we calculate the TOF of $Co_3O_4$. Evidently, contrarily to the $Co_3O_4$ and $CuMoO_4$ samples, all Co/Cu-X samples are highly catalytically active towards AB hydrolysis, which could be possibly due to the synergistic effect between $Co_3O_4$ and $CuMoO_4$. Based upon the literature, it has been observed that $Co^{2+}$ and $Cu^{2+}$ in the materials are not active towards the hydrolysis. However, AB in alkaline media acts as a reducing agent, which can reduce the $Co^{2+}$ and $Cu^{2+}$ to their metallic states, Co and Cu, and in turn acting as catalysts for AB hydrolysis. In the case of Co/Cu-X samples, the activity of Cu is much lower than that of Co, but $Cu^{2+}$ is easily reduced to its metallic state due to its relative high reduction potential ($Cu^{2+}$/Cu: 0.337 vs. SHE against $Co^{2+}$/Co:

-0.280 V vs. SHE).[34]

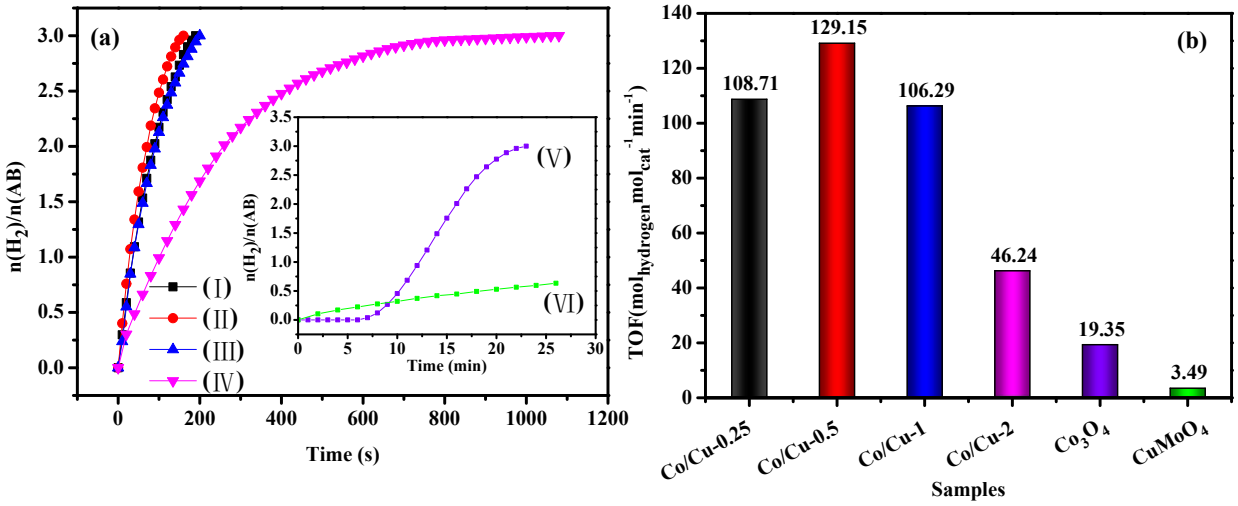


Figure 5 (a) Plot of $n(H_2)/n(AB)$ versus time for (Ⅰ) Co/Cu-0.25; (Ⅱ) Co/Cu-0.5; (Ⅲ) Co/Cu-1; (Ⅳ) Co/Cu-2; (Ⅴ) $Co_3O_4$; (Ⅵ) $CuMoO_4$;(b) the histogram of TOF for different samples.

The reducibility properties of the catalysts can be identified with the $H_2$-TPR profiles. As we discussed in the manuscript, the reducibility of the $Co_3O_4/CuMoO_4$ catalyst plays an important role in affecting their catalytic activity. Thus, $H_2$-TPR analysis is very crucial for us to understand the catalytic behavior in the present study. Figure 6 shows the reduction behavior of $Co_3O_4$, $CuMoO_4$ and Co/Cu-0.5 catalysts. For $Co_3O_4$, two prominent peaks of $H_2$ consumption are observed, with one centered at approximately 280 ℃, which is attributed to the reduction of $Co_3O_4$ to CoO, and the other peak of 370 ℃ due to the reduction of CoO to Co.[35,36] For $CuMoO_4$, the first peak corresponds to the complete reduction of CuO at ca. 290 ℃,[37] and the other two peaks appearing at 340 and 715 ℃, can be attributed to a two-step reduction process: $MoO_3 \rightarrow MoO_2$ and $MoO_2 \rightarrow Mo$. The chemical equations are listed as follows:[37]

$$CuMoO_4(s) + H_2(g) \rightarrow Cu(s) + MoO_3(s) + H_2O(g) \quad (1)$$

$$MoO_3(s) + H_2(g) \rightarrow MoO_2(s) + H_2O(g) \quad (2)$$

$$MoO_2(s) + 2H_2(g) \rightarrow Mo(s) + 2H_2O(g) \quad (3)$$

In our conditions, it was observed that CuO can be easily reduced to metallic copper compared to $Co_3O_4$. More interestingly, the TPR profiles of Co/Cu-0.5 indicated that all the reduction peaks shifted to the low temperature range under similar conditions, suggesting that the reduction process became "stronger", in turns indicating that the activity of the catalyst was greatly improved. When $Co_3O_4$ was combined with $CuMoO_4$ in these Co/Cu-X samples for the hydrolysis of AB, metallic Cu was firstly and rapidly formed on the surface of the Co/Cu-X samples, and these Cu acted as catalytic sites for the reduction of $Co^{2+}$,[35] resulting in metallic Co with much higher catalytic activity formed on the surface of the catalysts. As shown in Figure 7, Co(0) and Cu(0) were clearly detected in their corresponding XPS spectra after hydrolysis testing, confirming that Co and Cu metals or CoCu alloys were formed on the surface of Co/Cu-0.5 during AB hydrolysis process. Thus, the obtained Co/Cu-X samples exhibiting much higher TOF values than $Co_3O_4$ and $CuMoO_4$ could be due to the synergistic effect between $Co_3O_4$ and $CuMoO_4$.

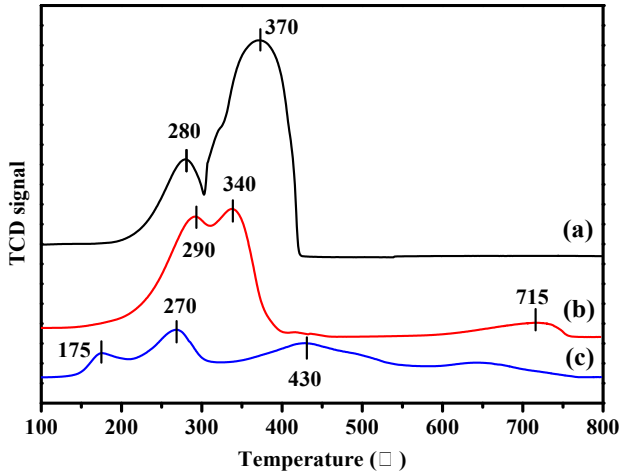


Figure 6 $H_2$-TPR profiles of the (a) $Co_3O_4$, (b) $CuMoO_4$ and (c) Co/Cu-0.5 samples.

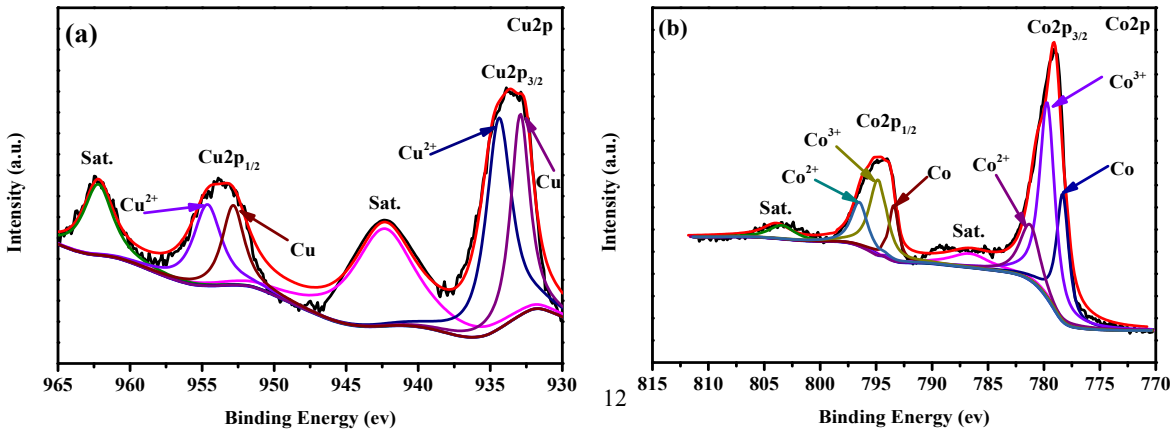

Figure 7 Deconvoluted high-resolution XPS spectra of Cu 2p (a) and Co 2p (b) for Co/Cu-0.5 after the hydrolysis testing.

There is a concern that Co/Cu-0.5 exhibit the highest catalytic activity in terms of TOF values among all these Co/Cu-X samples. As discussed above, the activity of $CuMoO_4$ is much lower than that of $Co_3O_4$ in AB hydrolysis. However, $CuMoO_4$ is indispensable in the catalysts because $CuMoO_4$ can induce the formation of active metallic Co in the reaction medium. Evidently, $Co_3O_4$ and $CuMoO_4$ play different roles in AB hydrolysis. Thus, there may be an optimized molar ratio of $Co_3O_4$ to $CuMoO_4$ to achieve the best catalytic performance for hydrolysis when they are combined together. Li et al. have once found that the CuCo alloys exhibits the highest catalytic activity in AB hydrolysis when the molar ratio of Co/(Co+Cu) is 0.70:1.[38] As for our Co/Cu-0.5 catalyst, the molar ratio of $Co_3O_4$ to $CuMoO_4$ is 1:1.89 and the corresponding molar ratio of Co/(Co+Cu) is about 0.61:1, which is close to optimal value in the literature. [38]

It is well-known that temperature has a significant effect on the hydrolysis reaction rate.[39] In this work, the hydrolysis of AB catalyzed by Co/Cu-0.5 were investigated in the temperature range of 20-40 °C. Figure 8(a) shows the hydrogen evolution curves obtained on Co/Cu-0.5 at various temperatures. The figure clearly shows that increasing the reaction temperature can effectively increase the reaction rate of AB hydrolysis. The apparent activity energy (Ea) values of AB hydrolysis were also calculated according to the Arrhenius equation:

$$\ln k = -Ea/(RT) + \ln A \qquad (4)$$

where A is the pre-exponential factor, Ea is the activation energy of the reaction, R is the molar gas constant, T is the reaction temperature (K) and k is the rate constant of the reaction.

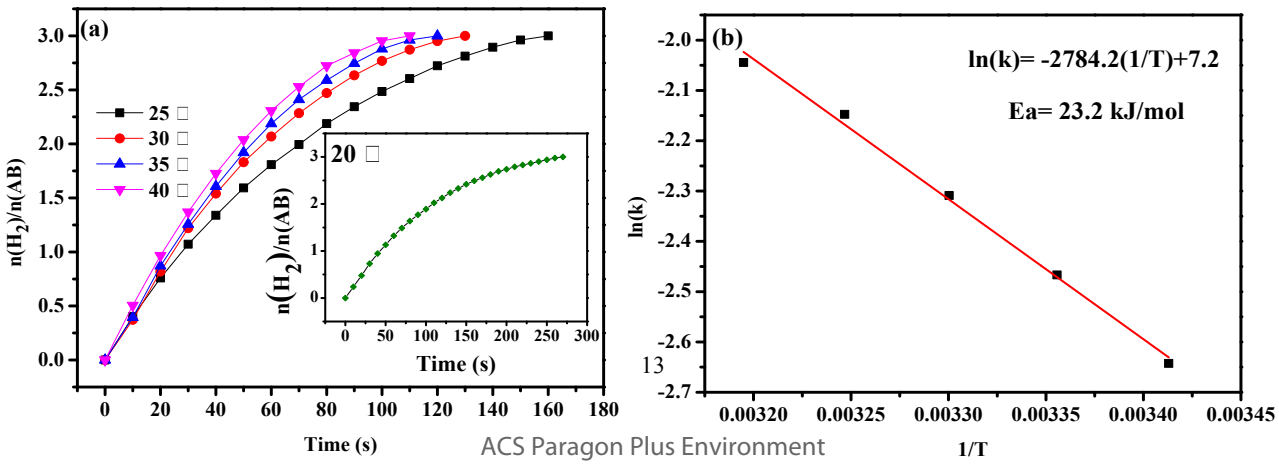

Figure 8 The effect of temperature on hydrolysis of AB catalyzed by Co/Cu-0.5 (a) Arrhenius plots of AB hydrolysis rates on Co/Cu-0.5 (b).

Based upon the above Arrhenius equation and Figure 8(b), the apparent activity energy value of AB hydrolysis on Co/Cu-0.5 was found to be 23.2 kJ $mol^{-1}$. The obtained Ea value of Co/Cu-0.5 was compared with those found in the literature for various catalyst materials (Table 1). The table clearly shows that the Co/Cu-0.5 is among the best in class, in terms of high TOF and low Ea values.

Table 1. Comparison of Co/Cu-0.5 with some representative catalysts reported in the literature.

| Catalysts | *TOF* ($min^{-1}$) | $E_a$ ( kJ $mol^{-1}$ ) | Reference |
|---|---|---|---|
| $Ni_{0.7}Co_{1.3}P$/GO | 153.9 | 43.2 | [19] |
| $Co_3O_4$/$CuMoO_4$ | 129.15 | 23.2 | This work |
| $Cu_{0.6}Ni_{0.4}Co_2O_4$ | 119.5 | 33.91 | [40] |
| $Cu_{0.72}Co_{0.18}Mo_{0.1}$ | 119 | 45 | [32] |
| Ni/ZIF-8 | 85.7 | /[a] | [41] |
| $Co_xCu_{1-x}Co_2O_4$@$Co_yCu_{1-y}Co_2O_4$ | 81.8 | 24.97 | [25] |
| CuCo/g-$C_3N_4$-1 | 75.1 | / | [42] |
| Hexagonal $CuCo_2O_4$ nanoplatelets | 73.4 | / | [43] |
| CoP | 72.7 | / | [44] |
| $Cu_{0.8}Co_{0.2}O$/Graphene oxide | 70.0 | 45.53 | [21] |
| $Ni_{0.9}Mo_{0.1}$/Graphene | 66.7 | 21.8 | [45] |
| $Co_{0.8}Cu_{0.2}MoO_4$ | 55.0 | 39.6 | [39] |
| CuCo/diamine-functionalized reduced graphene oxide | 51.5 | / | [46] |
| $NiCo_2O_4$/Ti | 50.1 | 17.5 | [47] |
| $CuCo_2O_4$(nanoplates)/Ti | 44.0 | 23.6 | [48] |

[a] No data were reported.

Figure 9(a) shows the mol $H_2$/mol AB versus time plots and the various amounts of Co/Cu-0.5 were plotted to investigate the effect of catalyst amount on the hydrogen generation rates. As expected, the hydrogen generation rates increased with the amount of Co/Cu-0.5. The logarithmic

plot (ln) of amount of Co/Cu-0.5 and hydrogen generation rate is presented in Figure 9(b), showing that the ln(rate) increased linearly with ln(catalyst amount) with a slope of 1.1 ± 0.03, i.e. the AB hydrolysis on Co/Cu-0.5 was found to be a first-order reaction with respect to catalyst mass.

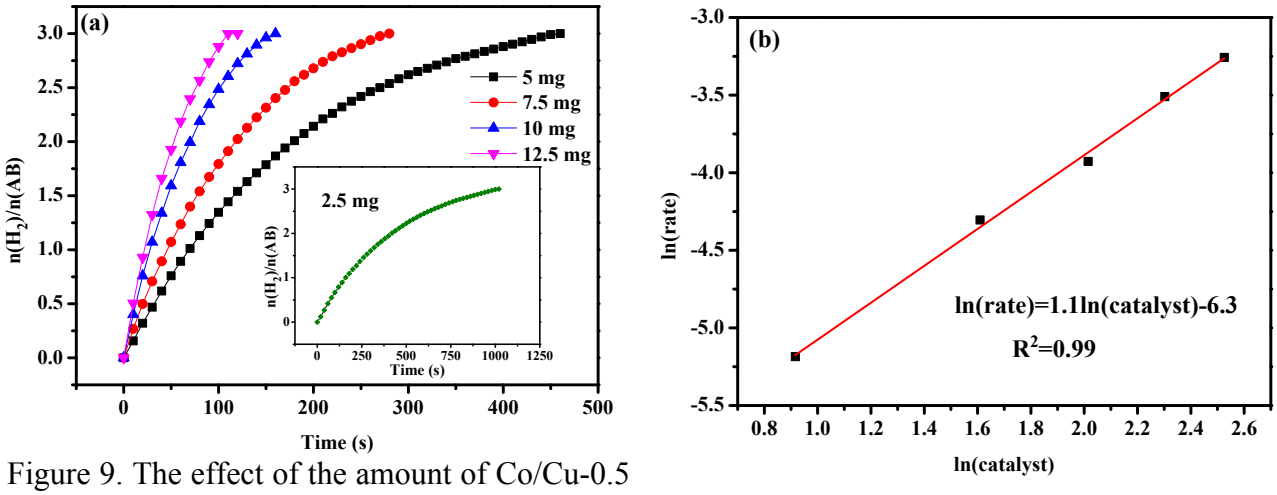


Figure 9. The effect of the amount of Co/Cu-0.5 on the hydrogen generation rates (a) and plot of ln(hydrogen generation rate) versus ln(catalyst amount)(b).

In order to have a better understanding of AB hydrolysis occurring on Co/Cu-0.5, the effect of AB concentrations on the AB hydrolysis on Co/Cu-0.5 was investigated. As shown in Figure 10, the amount of hydrogen generated on Co/Cu-0.5 increased with AB concentration. The logarithmic plot of AB concentration and rate constant are illustrated in the inset of Figure 10. The obtained slope of the linear ln(k) vs. ln(AB) plot was found to be 0.07 ± 0.004, indicating that the AB hydrolysis on Co/Cu-0.5 is close to a zero-order kinetics reaction with respect to AB concentration.

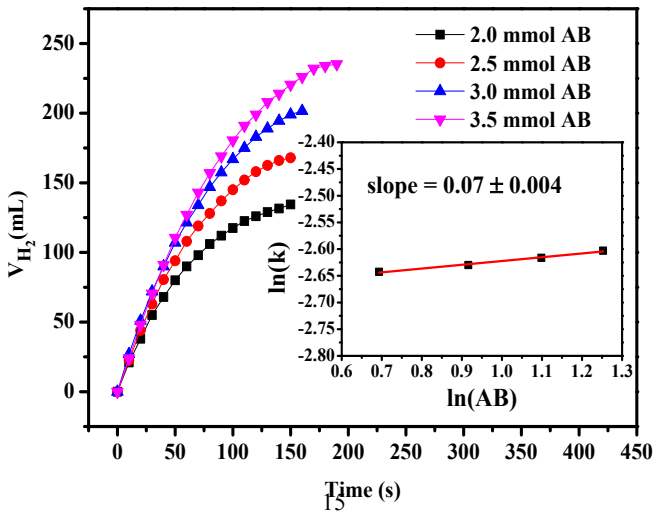

Figure 10 Effect of AB concentrations on hydrogen generation and plot of ln(hydrogen generation rate, k) versus ln(AB concentrations) (inset).

Finally, the stability and reusability of the Co/Cu-0.5 catalyst was investigated and the results were shown in Figure 11. As can be seen, the catalyst slightly loses its catalytic activity after 5 catalytic run. However, the molar ratio of hydrogen to AB can still reach 3 at 5$^{th}$ catalytic run, demonstrating that the complete hydrogen release can be achieved. These observations indicate that our Co/Cu-0.5 catalyst possesses relatively high stability and good reusability. We have checked the used Co/Cu-0.5 catalyst with XRD and the result is displayed in Figure S3. Clearly, CoCu alloys are formed in the used catalysts, which is in line with the XPS results. As discussed above, CoCu alloys are generated by the co-reduction of active spices with AB.

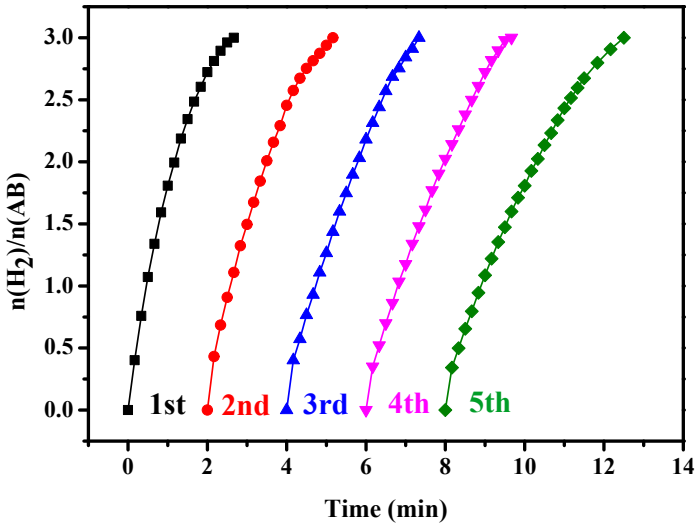


Figure 11 Hydrogen evolution curves at different catalytic cycles.

## CONCLUSIONS

In summary, $Co_3O_4/CuMoO_4$ hybrid microflowers composed of nanorods were successfully synthesized by a hydrothermal approach, followed by a calcination process. The nanorods in the microflowers clearly displayed a rough, turf and rich particle boundaries, made of irregular small nanoparticles. The element mapping results demonstrated that $Co_3O_4/CuMoO_4$ hybrids were formed

in these nanorods. The obtained $Co_3O_4$/$CuMoO_4$ hybrid exhibited outstanding catalytic activity towards the AB hydrolysis due to the synergistic effect between $Co_3O_4$ and $CuMoO_4$. Among all the as-prepared Co/Cu samples, Co/Cu-0.5 exhibited the best catalytic activity with a TOF value of 129.15 $mol_{hydrogen}mol_{cat}^{-1}$ $min^{-1}$, which is one of the best noble-mental-free catalysts for AB hydrolysis in class. Our findings also showed that the obtained Co/Cu-0.5 could be a promising catalyst of AB hydrolysis for practical hydrogen production.

## ASSOCIATED CONTENT

### Supporting Information

$N_2$ adsorption-desorption isotherms of different samples can be seen in the support information. This material is available free of charge via the Internet at http://pubs.acs.org.

## AUTHOR INFORMATION

Author Contributions

The manuscript was written through contributions of all authors. All authors have given approval to the final version of the manuscript.

### Notes

The authors declare no competing financial interest.

## ACKNOWLEDGEMENT

This work was supported by the Natural Science Foundation of Guangdong Province (No. 2018A030313859), the Major Project of Fundamental and Application Research of the Department of Education of Guangdong Province (No. 2017KZDXM079), the Science & Technology project of Huizhou City (No. 2017C0412028), the Natural Science Foundation of Huizhou University (Nos. 20180927172750326 and HZU201714), and the Science and Technology Innovation Foundation for College Student of Guangdong Province (PDJH2019b0470).

## REFERENCES

[1] Schlapbach, L.; Züttel, A. Hydrogen-storage materials for mobile applications. Nature **2001**,

414, 353-358. DOI:10.1038/35104634.

[2] Ding, J.; Ji, S.; Wang, H.; Key, J.; Brett, D. J. L.; Wang, R. Nano-engineered intrapores in nanoparticles of PtNi networks for increased oxygen reduction reaction activity. J. Power Sources **2018**, 374, 48-54. DOI:10.1016/j.jpowsour.2017.11.002.

[3] Wang, X.; Liao, J.; Li, H.; Wang, H.; Wang, R.; Pollet, B. G.; Ji, S. Highly active porous Co-B nanoalloy synthesized on liquid-gas interface for hydrolysis of sodium borohydride. Int. J. Hydrogen Energy **2018**, 43, 17543-17555. DOI:10.1016/j.ijhydene.2018.07.147.

[4] Wang, R.; Wang, K.; Wang, Z.; Song, H.; Wang, H.; Ji, S. Pig bones derived N-doped carbon with multi-level pores as electrocatalyst for oxygen reduction. J. Power Sources **2015**, 297, 295-301. DOI:10.1016/j.jpowsour.2015.07.107.

[5] De Bruijn, F. A. Hydrogen as a Future Energy Carrier. Edited by Andreas Züttel, Andreas Borgschulte, and Louis Schlapbach. ChemSusChem **2008**, 1, 782-783. DOI:10.1002/cssc.200800119.

[6] Feng, K.; Zhong, J.; Zhao, B.; Zhang, H.; Xu, L.; Sun, X.; Lee, S. T. $Cu_xCo_{1-x}O$ Nanoparticles on Graphene Oxide as A Synergistic Catalyst for High-Efficiency Hydrolysis of Ammonia-Borane. Angew. Chem. Int. Ed. **2016**, 55, 11950-11954. DOI:10.1002/anie.201604021.

[7] Şahin, Ö.; Karakaş, D. E.; Kaya, M.; Saka, C. The effects of plasma treatment on electrochemical activity of Co-B-P catalyst for hydrogen production by hydrolysis of $NaBH_4$. J. Energy Inst. **2017**, 90, 466-475. DOI:10.1016/j.ijhydene.2013.09.098.

[8] Larichev, Y. V.; Netskina, O. V.; Komova, O. V.; Simagina, V. I. Comparative XPS study of $Rh/Al_2O_3$ and $Rh/TiO_2$ as catalysts for $NaBH_4$ hydrolysis. Int. J. Hydrogen Energy **2010**, 35, 6501-6507. DOI:10.1016/j.ijhydene.2010.04.048.

[9] Keçeli, E.; Özkar, S. Ruthenium(III) acetylacetonate: A homogeneous catalyst in the hydrolysis of sodium borohydride. J. Mol. Catal. A Chem. **2008**, 286, 87-91. DOI: 10.1016/j.molcata.2008.02.008.

[10] Patel, N.; Patton, B.; Zanchetta, C.; Fernandes, R.; Guella, G.; Kale, A.; Miotello, A. Pd-C

powder and thin film catalysts for hydrogen production by hydrolysis of sodium borohydride. Int. J. Hydrogen Energy **2008**, 33, 287-292. DOI:10.1016/j.ijhydene.2007.07.018.

[11] Liu, H.; Yu, Y.; Yang, W.; Lei, W.; Gao, M.; Guo, S. High-density defects on PdAg nanowire networks as catalytic hot spots for efficient dehydrogenation of formic acid and reduction of nitrate. Nanoscale **2017**, 9, 9305-9309. DOI:10.1039/c7nr03734a.

[12] Liu, H.; Huang, B.; Zhou, J.; Wang, K.; Yu, Y.; Yang, W.; Guo, S. Enhanced electron transfer and light absorption on imino polymer capped PdAg nanowire networks for efficient room-temperature dehydrogenation of formic acid. J. Mater. Chem. A **2018**, 6, 1979-1984. DOI: 10.1039/c7ta10963f.

[13] Gao, M.; Yang, W.; Yu, Y. Monodisperse PtCu alloy nanoparticles as highly efficient catalysts for the hydrolytic dehydrogenation of ammonia borane. Int. J. Hydrogen Energy **2018**, 43, 14293-14300. DOI:10.1016/j.ijhydene.2018.05.158.

[14] Xu, D.; Zhang, H.; Wei, Y. Hydrogen generation from hydrolysis of alkaline sodium borohydride solution using Pt/C catalyst. Catal. Commun. **2007**, 8, 1767-1771. DOI: 10.1016/j.catcom.2007.02.028.

[15] Lee, J.; Kong, K. Y.; Jung, C. R.; Cho, E.; Yoon, S. P.; Han, J.; Lee, T.-G.; Nam, S. W. A structured Co-B catalyst for hydrogen extraction from $NaBH_4$ solution. Catal. Today **2007**, 120, 305-310. DOI:10.1016/j.cattod.2006.09.019.

[16] Shen, M.; Liu, H.; Yu, C.; Yin, Z.; Muzzio, M.; Li, J.; Xi, Z.; Yu, Y.; Sun, S. Room-temperature Chemoselective Reduction of 3-nitrostyrene to 3-vinylaniline by Ammonia Borane over Cu Nanoparticles. J. Am. Chem. Soc. **2018**, 140, 16460-16463. DOI:10.1021/jacs.8b11303.

[17] Gao, M.; Yu, Y.; Yang, W.; Li, J.; Xu, S.; Feng, M.; Li, H. Ni nanoparticles supported on graphitic carbon nitride as visible light catalysts for hydrolytic dehydrogenation of ammonia borane. Nanoscale **2019**, 11, 3506-3513. DOI:10.1039/c8nr09005j.

[18] Akdim, O.; Demirci, U. B.; Miele, P. A bottom-up approach to prepare cobalt-based bimetallic

supported catalysts for hydrolysis of ammonia borane. Int. J. Hydrogen Energy **2013**, 38, 5627-5637. DOI:10.1016/j.ijhydene.2013.02.110.

[19] Hou, C.-C.; Li, Q.; Wang, C.-J.; Peng, C.-Y.; Chen, Q.-Q.; Ye, H.-F.; Fu, W.-F.; Che, C.-M.; López, N.; Chen, Y. Ternary Ni-Co-P nanoparticles as noble-metal-free catalysts to boost the hydrolytic dehydrogenation of ammonia-borane. Energy Environ. Sci. **2017**, 10, 1770-1776. DOI: 10.1039/c7ee01553d.

[20] Li, C.; Wang, D.; Wang, Y.; Li, G.; Hu, G.; Wu, S.; Cao, Z.; Zhang K. Enhanced catalytic activity of the nanostructured Co-W-B film catalysts for hydrogen evolution from the hydrolysis of ammonia borane. J. Colloid Interface Sci. **2018**, 524, 25-31. DOI:10.1016/j.jcis.2018.03.085.

[21] Feng, K.; Zhong, J.; Zhao, B.; Zhang, H.; Xu, L.; Sun, X.; Lee, S. T. $Cu_xCo_{1-x}O$ Nanoparticles on Graphene Oxide as A Synergistic Catalyst for High-Efficiency Hydrolysis of Ammonia-Borane. Angew. Chem. Int. Ed. **2016**, 55, 11950-11954. DOI:10.1002/anie.201604021.

[22] Yamada, Y.; Yano, K.; Fukuzumi, S. Catalytic application of shape-controlled $Cu_2O$ particles protected by $Co_3O_4$nanoparticles for hydrogen evolution from ammonia borane. Energy Environ. Sci. **2012**, 5, 5356-5363. DOI:10.1039/c1ee02639a.

[23] Yen, H.; Kleitz, F. High-performance solid catalysts for $H_2$ generation from ammonia borane: progress through synergetic Cu-Ni interactions. J. Mater. Chem. A **2013**, 1, 14790-14796. DOI: 10.1039/c3ta13681g.

[24] Peng, C.-Y.; Hou, C.-C.; Chen, Q.-Q.; Wang, C.-J.; Lv, X.-J.; Zhong, J.; Fu, W.-F.; Che, C.-M.; Chen, Y. $Cu(OH)_2$ supported on $Fe(OH)_3$ as a synergistic and highly efficient system for the dehydrogenation of ammonia-borane. Sci. Bull. **2018**, 63, 1583-1590. DOI:10.1016/j.scib.2018.11.003.

[25] Lu, D.; Li, J.; Lin, C.; Liao, J.; Feng, Y.; Ding, Z.; Li, Z.; Liu, Q.; Li, H. A Simple and Scalable Route to Synthesize $Co_xCu_{1-x}Co_2O_4$@$Co_yCu_{1-y}Co_2O_4$ Yolk-Shell Microspheres, A High-Performance Catalyst to Hydrolyze Ammonia Borane for Hydrogen Production. Small **2019**, 15, 1805460(1-9). DOI:10.1002/smll.201805460.

[26] Fernandes, R.; Patel, N.; Miotello, A.; Calliari, L. Co – Mo – B – P Alloy with Enhanced Catalytic Properties for $H_2$ Production by Hydrolysis of Ammonia Borane. Top. Catal. **2012**, 55, 1032-1039. DOI:10.1007/s11244-012-9889-9.

[27] Zhou, M.; Lu, F.; Shen, X.; Xia, W.; He, H.; Zeng, X. One-pot construction of three dimensional $CoMoO_4/Co_3O_4$ hybrid nanostructures and their application in supercapacitors. J. Mater. Chem. A **2015**, 3, 21201-21210. DOI:10.1039/c5ta05658f.

[28] Zhang, W.; Yin, J.; Min, F.; Jia, L.; Zhang, D.; Zhang, Q.; Xie, J. Preparation and photoluminescence properties of $MMoO_4$ (M = Cu, Ni, Zn) nano-particles synthesized via electrolysis. J. Mol. Struct. **2017**, 1127, 777-783. DOI:10.1016/j.molstruc.2016.08.020.

[29] He, G.; Qiao, M.; Li, W.; Lu, Y.; Zhao, T.; Zou, R.; Li, B.; Darr, J. A.; Hu, J.; Titirici, M. M.; Parkin, I. P. S, N-Co-Doped Graphene-Nickel Cobalt Sulfide Aerogel: Improved Energy Storage and Electrocatalytic Performance. Adv. Sci. **2017**, 4, 1600214 (1-10). DOI:10.1002/advs.201600214.

[30] Cui, J.; Zhang, X.; Tong, L.; Luo, J.; Wang, Y.; Zhang, Y.; Xie, K.; Wu Y. A facile synthesis of mesoporous $Co_3O_4/CeO_2$ hybrid nanowire arrays for high performance supercapacitors. J. Mater. Chem. A **2015**, 3, 10425-10431. DOI:10.1039/c5ta00860c.

[31] Cheng, H.; Kamegawa, T.; Mori, K.; Yamashita, H. Surfactant-free nonaqueous synthesis of plasmonic molybdenum oxide nanosheets with enhanced catalytic activity for hydrogen generation from ammonia borane under visible light. Angew. Chem. Int. Ed. **2014**, 53, 2910-2914. DOI: 10.1002/ange.201309759.

[32] Yao, Q.; Yang, K.; Hong, X.; Chen, X.; Lu, Z.-H. Base-promoted hydrolytic dehydrogenation of ammonia borane catalyzed by noble-metal-free nanoparticles. Catal. Sci. Technol. **2018**, 8, 870-877. DOI:10.1039/c7cy02365k.

[33] Du, X.; Yang, C.; Zeng, X.; Wu, T.; Zhou, Y.; Cai, P.; Cheng, G.; Luo, W. Amorphous NiP supported on rGO for superior hydrogen generation from hydrolysis of ammonia borane. Int. J. Hydrogen Energy **2017**, 42, 14181-14187. DOI:10.1016/j.ijhydene.2017.04.052.

[34] Li, C.; Zhou, J.; Gao, W.; Zhao, J.; Liu, J.; Zhao, Y.; Wei, M.; Evans, D. G.; Duan, X. Binary Cu–Co catalysts derived from hydrotalcites with excellent activity and recyclability towards $NH_3BH_3$ dehydrogenation. J. Mater. Chem. A **2013**, 1, 5370-5376. DOI:10.1039/c3ta10424a.

[35] Bulavchenko, O. A.; Gerasimov, E. Y.; Afonasenko, T. N. Reduction of double manganese-cobalt oxides: in situ XRD and TPR study. Dalton Trans. **2018**, 47, 17153-17159. DOI:10.1039/c8dt04137g.

[36] Fei, T.; Chen, M.; Li, G.; Yang, T.; Xu, T.; Hang, Y.; Yao, W.; Santhanagopalan, S.; Meng, D. D.; Zhu, Y. High combustion activity of $CH_4$ and catalluminescence properties of CO oxidation over porous $Co_3O_4$ nanorods. Appl. Catal. B: Environ. **2011**, 110, 133-140. DOI: 10.1016/j.apcatb.2011.08.035.

[37] Ming, Z.; Wang, J.; Wei, L.; Zhou, M. Preparation and reduction behavior of Mo-Cu powders by Sol-Gel. J. Phys. Conf. Ser. **2009**, 188, 2-6. DOI:10.1088/1742-6596/188/1/012020.

[38] Li, J.; Zhu, Q.-L.; Xu, Q. Non-noble bimetallic CuCo nanoparticles encapsulated in the pores of metal-organic frameworks: synergetic catalysis in the hydrolysis of ammonia borane for hydrogen generation. Catal. Sci. Technol. **2015**, 5, 525-530. DOI:10.1039/c4cy01049c.

[39] Liao, J.; Lu, D.; Diao, G.; Zhang, X.; Zhao, M.; Li, H. $Co_{0.8}Cu_{0.2}MoO_4$ Microspheres Composed of Nanoplatelets as a Robust Catalyst for the Hydrolysis of Ammonia Borane. ACS Sustainable Chem. Eng. **2018**, 6, 5843-5851. DOI:10.1021/acssuschemeng.7b03994.

[40] Lu, D.; Liao, J.; Zhong, S.; Leng, Y.; Ji, S.; Wang, H.; Wang, R.; Li, H. $Cu_{0.6}Ni_{0.4}Co_2O_4$ nanowires, a novel noble-metal-free catalyst with ultrahigh catalytic activity towards the hydrolysis of ammonia borane for hydrogen production. Int. J. Hydrogen Energy, **2018**, 43, 5541-5550. DOI:10.1016/j.ijhydene.2018.01.129.

[41] Wang, C.; Tuninetti, J.; Wang, Z.; Zhang, C.; Ciganda, R.; Salmon, L.; Moya, S.; Ruiz, J.; Astruc, D. Hydrolysis of Ammonia-Borane over Ni/ZIF-8 Nanocatalyst: High Efficiency, Mechanism, and Controlled Hydrogen Release. J. Am. Chem. Soc. **2017**, 139, 11610-11615. DOI: 10.1021/jacs.7b06859.

[42] Zhang, H.; Gu, X.; Liu, P.; Song, J.; Cheng, J.; Su, H. Highly efficient visible-light-driven catalytic hydrogen evolution from ammonia borane using non-precious metal nanoparticles supported by graphitic carbon nitride. J. Mater. Chem. A **2017**, 5, 2288-2296. DOI: 10.1039/c6ta08987a.

[43] Liao, J.; Feng, Y.; Wu, S.; Ye, H.; Zhang, J.; Zhang, X.; Xie F.; Li, H. Hexagonal $CuCo_2O_4$ Nanoplatelets, a Highly Active Catalyst for the Hydrolysis of Ammonia Borane for Hydrogen Production. Nanomaterials **2019**, 9, 360 (1-11). DOI:10.3390/nano9030360.

[44] Fu, Z. C.; Xu, Y.; Chan, S. L.; Wang, W. W.; Li, F.; Liang, F.; Chen, Y.; Lin, Z. S.; Fu, W. F.; Che, C. M. Highly efficient hydrolysis of ammonia borane by anion (-OH, F-, Cl-)-tuned interactions between reactant molecules and CoP nanoparticles. Chem. Commun. **2017**, 53, 705-708. DOI:10.1039/c6cc08120g.

[45] Yao, Q.; Lu, Z.-H.; Huang, W.; Chen, X.; Zhu, J. High Pt-like activity of the Ni-Mo/graphene catalyst for hydrogen evolution from hydrolysis of ammonia borane. J. Mater. Chem. A **2016**, 4, 8579-8583. DOI:10.1039/c6ta02004f.

[46] Song, F. Z.; Zhu, Q. L.; Yang, X. C.; Xu, Q. Monodispersed CuCo Nanoparticles Supported on Diamine-Functionalized Graphene as a Non-noble Metal Catalyst for Hydrolytic Dehydrogenation of Ammonia Borane. ChemNanoMat **2016**, 2, 942-945. DOI:10.1002/cnma.201600198.

[47] Liao, J.; Li, H.; Zhang, X.; Feng, K.; Yao, Y. Fabrication of a Ti-supported $NiCo_2O_4$ nanosheet array and its superior catalytic performance in the hydrolysis of ammonia borane for hydrogen generation. Catal. Sci. Technol. **2016**, 6, 3893-3899. DOI:10.1039/c5cy01542a.

[48] Liu, Q.; Zhang, S.; Liao, J.; Feng, K.; Zheng, Y.; Pollet, B. G.; Li, H. $CuCo_2O_4$ nanoplate film as a low-cost, highly active and durable catalyst towards the hydrolytic dehydrogenation of ammonia borane for hydrogen production. J. Power Sources **2017**, 355, 191-198. DOI:10.1016/j.jpowsour.2017.04.057.

## For Table of Contents Use Only

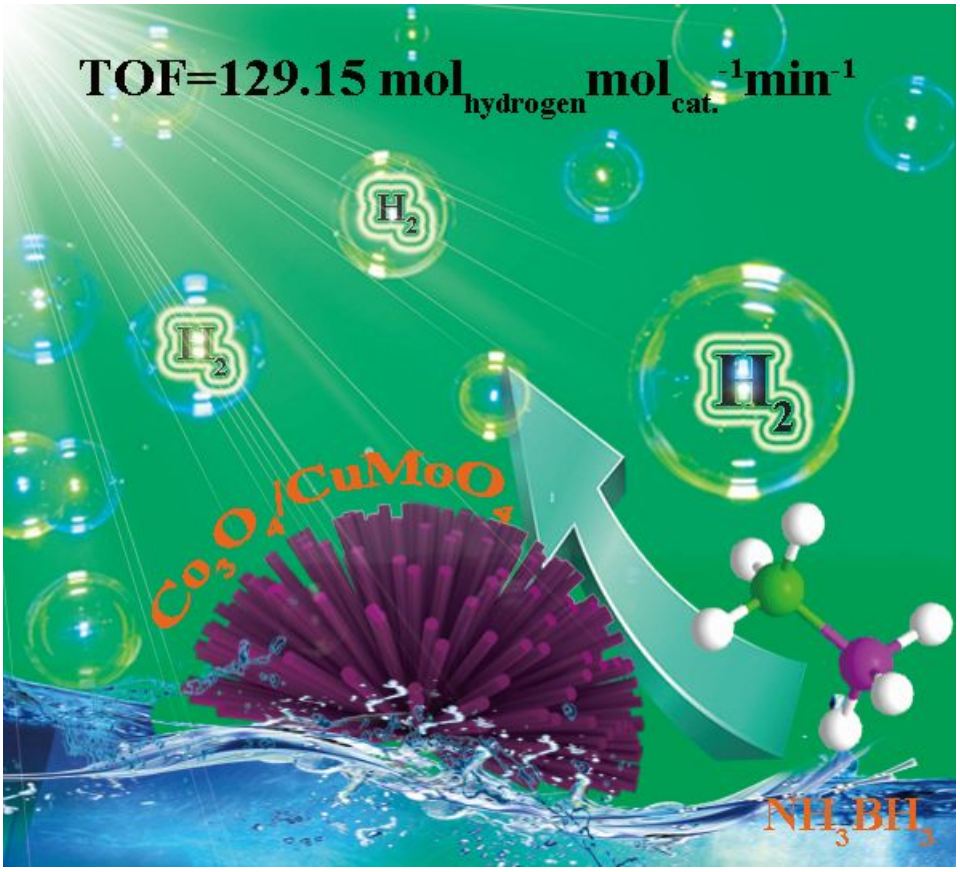


**$Co_3O_4$/$CuMoO_4$ hybrid microflowers composed of nanorods can be used in the catalytic hydrolysis of ammonia borane for fast hydrogen production**